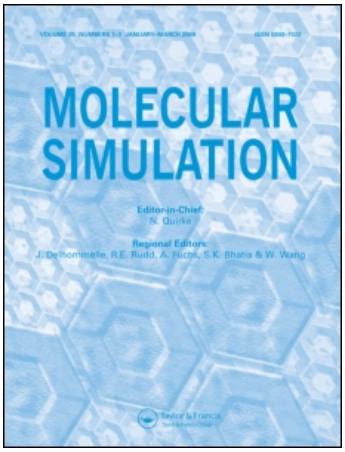

Molecular Simulation

Publication details, including instructions for authors and subscription information:
http://www.informaworld.com/smpp/title~content=t713644482

Protein dynamics control of electron transfer in reaction centers from *Rps. viridis*

E. S. Medvedev[a]; A. I. Kotelnikov[a]; N. S. Goryachev[a]; B. L. Psikha[a]; J. M. Ortega[b]; A. A. Stuchebrukhov[c]
[a] The Institute of Problems of Chemical Physics, Russian Academy of Sciences, Chernogolovka, Russia [b] Instituto de Bioquimica Vegetal y Fotosintesis, Universidad de Seville-CSIC, Seville, Spain [c] Department of Chemistry, University of California, Davis, CA, USA

To cite this Article Medvedev, E. S. , Kotelnikov, A. I. , Goryachev, N. S. , Psikha, B. L. , Ortega, J. M. and Stuchebrukhov, A. A.(2006) 'Protein dynamics control of electron transfer in reaction centers from *Rps. viridis*', Molecular Simulation, 32: 9, 735 — 750
To link to this Article: DOI: 10.1080/08927020600880802
URL: http://dx.doi.org/10.1080/08927020600880802

Molecular Simulation, Vol. 32, No. 9, 15 August 2006, 735–750

Protein dynamics control of electron transfer in reaction centers from *Rps. viridis*

E. S. MEDVEDEV†, A. I. KOTELNIKOV†, N. S. GORYACHEV†, B. L. PSIKHA†, J. M. ORTEGA‡ and A. A. STUCHEBRUKHOV¶*

†The Institute of Problems of Chemical Physics, Russian Academy of Sciences, 142432 Chernogolovka, Russia
‡Instituto de Bioquimica Vegetal y Fotosintesis, Universidad de Seville–CSIC, E-41092 Seville, Spain
¶Department of Chemistry, University of California, Davis, CA 95616, USA

(Received April 2006; in final form May 2006)

Electron transfer (ET) in the reaction center from *Rhodopseudomonas viridis* has been studied experimentally by our group in the range of temperatures of 153–295 K. The kinetics of ET reaction from the proximal heme of cytochrome to the special pair was found to be non-exponential. The degree of non-exponentiality strongly depends on temperature, with increasing non-exponentiality at lower temperatures. Here, the experimental kinetic data for ET are analyzed in the frames of a theoretical Sumi–Marcus-type model, which allows establishing a connection between the observed kinetics and local structural dynamics of the protein in a close vicinity of the donor and acceptor sites. The phenomenological model subdivides the multi-time-scale dynamics of the protein into two groups: fast and slow. The division is determined by the rate of ET, which is dynamically controlled by the slow modes of the protein medium. The slow modes are described by a phenomenological collective coordinate X, for which a diffusion type of dynamics is assumed. The analysis of the temperature dependence of the kinetic curves for ET allows a complete characterization of the slow time-scale protein dynamics: we find the corresponding activation barrier for the dynamics of X, around 0.5 eV and the exponential pre-factor, which is in the range of 10^{-16} s. The pre-exponential factor is lower than is expected for a typical activation process described by the transition state theory. We discuss the nature of the collective modes X, the nature of its activation barrier (breaking of hydrogen bonds) and possible explanations for a low-pre-exponential factor of its dynamics. The main conclusion of the paper is that the kinetics of ET at low-temperatures can be used as a probe of protein structural dynamics in the microsecond time-scale, the time-scale that is not easily accessible by the computer simulations methods and can be complementary to other experimental techniques.

Keywords: Electron transfer; Protein dynamics; Reaction centers; Non-exponential kinetics

1. Introduction

For an electron transfer (ET) reaction to occur, the thermal motion of the medium surrounding electron donor and acceptor is necessary. In case of biological ET, the medium is a protein matrix in which donor and acceptor complexes are imbedded, thus protein dynamics is a key factor for ET in proteins. Can ET reaction then be used as a probe of protein dynamics? In recent years, several groups explored this question experimentally [1–10].

In this paper, we develop theory and show how the analysis of the temperature dependence of the kinetics of ET allows one to get insights into details of the corresponding protein structural dynamics.

A great number of examples of ET proteins is provided by biological energy generating machinery, of which the reaction center of photosynthesis is one prominent example. Earlier, the ET from the proximal heme c-559 to the special pair in the reaction center from *Rhodopseudomonas viridis* has been investigated experimentally by our group in the range of temperatures of 153–295 K. The kinetics of ET reaction from the proximal heme of cytochrome to the special pair was found to be non-exponential. The degree of non-exponentiality strongly depends on temperature, with increasing non-exponentiality at lower temperatures, as one approaches the glass transition temperature, T_g, where the protein structural dynamics slows down.

*Corresponding author. Fax: + 1-530-752-8995. Email: aastuchebrukhov@ucdavis.edu

Molecular Simulation
ISSN 0892-7022 print/ISSN 1029-0435 online © 2006 Taylor & Francis
http://www.tandf.co.uk/journals
DOI: 10.1080/08927020600880802

At room temperature, in this as in many other biological ET systems [11,12], the kinetics is almost single-exponential. In such a regime, the protein medium dynamics is much faster than ET and the ET rate is not sensitive to the protein dynamics *per se*, as long as it is sufficiently fast; instead, only the energetic parameters of this dynamics enter into the rate expression in terms of reorganization energy, driving force and electronic coupling, according to the standard Marcus theory. However, as the protein dynamics slows down at low-temperatures, it begins to bottleneck the ET. In such conditions, the ET occurs from many quite different conformations of the protein and the kinetics of the reaction becomes multi-exponential. It is in these conditions, one can say that the ET is controlled by the protein medium dynamics *per se* and the non-exponential kinetics can be used as a probe of the protein dynamics. Once the parameters of the dynamics are determined at low-temperatures and a theory is available for its temperature dependence, the conclusions can be drawn on the protein dynamics not only at low, but at room temperature as well.

Protein dynamics is multi-time-scale in nature, with different types of motions occurring on a femtosecond to a millisecond, or even slower time-scales. The slow complex collective motions of the protein involving structural rearrangements are difficult to characterize and any probe of such dynamics is of significant value. Only few studies where ET is used as a probe are described in the literature (Kotelnikov's [1–3], Nienhaus' [4,5] and Gray-Winkler's [6–10] studies).

Here, the experimental ET kinetic data are analyzed in the frames of a theoretical Sumi–Marcus-type model [13], which allows establishing a connection between the observed kinetics and structural dynamics of the protein† [14–18]. The phenomenological model subdivides the multi-time-scale dynamics of the protein into two groups: fast and slow. The division is determined by the rate of ET, which is dynamically controlled by the slow modes of the protein medium. The slow modes are described by a phenomenological collective coordinate X, for which a diffusion type of dynamics is assumed. The analysis of the temperature dependence of the ET kinetic curves allows a complete characterization of the slow time-scale protein dynamics: we find the corresponding activation barrier for the dynamics of X around 0.5 eV and the exponential pre-factor, which is in the range of 10^{-16} s. The pre-exponential factor is lower than is expected for a typical activation process described by the transition state theory. We discuss the nature of the collective mode X, the nature of its activation barrier (breaking of hydrogen bonds) and possible explanations for a low-pre-exponential factor of its dynamics. The main conclusion of the paper is that the ET kinetics at low-temperatures can be used as a probe of protein structural dynamics in the microsecond time-scale, the time-scale which is not easily accessible by the computer simulations methods and can be complementary to other experimental techniques, e.g. Mössbauer [19,20] and optical [21–24] spectroscopy.

The plan of the paper is as follows. In the next Section 2, we describe a theoretical model that will be used for the analysis of kinetic data, Section 3 will describe the fitting procedure to extract dynamic parameters from the kinetic curves, Section 4 gives a comparison with other methods used to monitor the dynamics of proteins and viscous solutions and the last Section 5 will discuss results and summarize the findings.

2. Model

We assume that all modes of the protein coupled to the ET are divided into three groups: one quantum mode q, to describe quantum effects, a classical "fast" collective coordinate x and a classical "slow" collective coordinate X. The fast and slow classical coordinates are some collective independent coordinates of the protein that presumably describe different types of motions of the protein—the first refers to dynamics of various bonds of the protein and the second is related to more macroscopic, structural dynamics. Therefore, they relate to different time-scales. However, the description is entirely phenomenological and within this theory, we can only speculate on what type of motions of the protein they may correspond.

If both x and X were fast enough, the rate of ET would be expressed in the standard form of the Marcus theory, with quantum corrections due to quantum mode q, in terms of the reorganization energy for the entire system, driving force and electronic coupling.

We assume, however, a possibility that X can be slow and therefore the setup of the model is as follows. We assume that the reaction can occur at different conformations of the protein that correspond to different values of X. For each such conformation, the rate of the reaction will be written as

$$k(X) = \frac{H_{\mathrm{DA}}^2}{\hbar}\sqrt{\frac{\pi}{\lambda_2 k_{\mathrm{B}} T}}\exp\left[-\frac{(\lambda_1 + \Delta G(X))^2}{4\lambda_2 k_{\mathrm{B}} T}\right] \quad (1)$$

This formula looks like a standard classical ET rate expression, but in fact it takes into account quantum effects by introducing two reorganization energies, λ_1 and λ_2. This is of course, an approximation, but a good one, which works well in a wide range of ΔG variation around the maximum of the rate. This formula was derived by Lee *et al.* [25]. Thus, except for some generalization of the reorganization energy, this is a standard expression for the rate, with a driving force that is different for different conformations of the protein X, thus we have $\Delta G(X)$.

†Similar ideas extending the original Zusman model [14] to include a non-diffusive mode were developed by Ovchinnikova [15], Alexandrov [16], Helman [17], Agmon and Hopfield [18] and others.

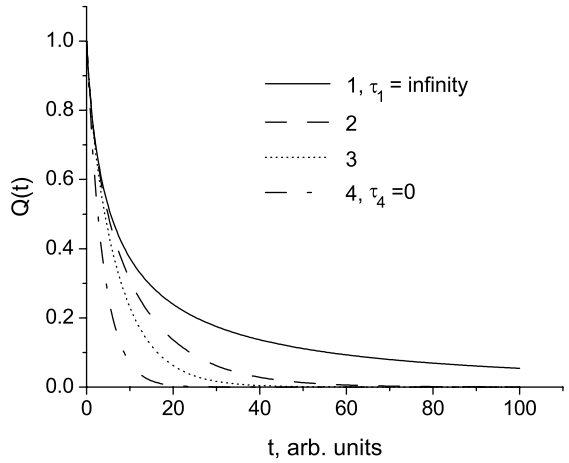

Figure 1. Schematic behavior of the kinetic curves at various relaxation times $\tau_1 > \tau_2 > \tau_3 > \tau_4$.

Expression (1) ignores a possible dependence of the matrix element H_{DA} on the conformational coordinate [26–32]. Such dependence may arise due to conformational changes in the medium separating the donor and acceptor sites. On the contrary, the driving force is modulated by conformational fluctuations in an immediate vicinity of the donor and acceptor centers, i.e. different types of conformational motions are responsible for the effect on the electronic coupling and the driving force. The effect on H_{DA} arises only under special conditions specified in the above-cited papers whereas the effect on ΔG is very general. In this paper, we neglect the former following the original approach by Sumi and Marcus.

The two λ's in equation (1) are:

$$\lambda_1 = \lambda_{cl} + \lambda_q, \quad \lambda_2 = \lambda_{cl} + \frac{\hbar\omega_q\lambda_q}{2k_BT}\coth\left(\frac{\hbar\omega_q}{2k_BT}\right) \qquad (2)$$

where λ_q and λ_{cl} are reorganization energies of the quantum and classical modes, respectively and ω_q is the frequency characterizing the quantum mode (assumed to be high compared with $k_BT/\hbar$). We now need to specify how the driving force depends on X.

The free energy profile for X in the reagents state is written as

$$V(x) = \frac{1}{2}X^2, \qquad (3)$$

that is the slow collective coordinate X is formally described as one of the oscillators of the medium. Then, the driving force for the reaction at given X is [13]

$$\Delta G(X) = \Delta G^0 + V(X - X_0) - V(X)$$
$$= \Delta G^0 + \lambda_X - \sqrt{2\lambda_X}X \qquad (4)$$

where $X_0 = \sqrt{2\lambda_X}$ is the equilibrium value in the products state and λ_X is the reorganization energy of X.

The next step is to specify how the collective coordinate X is changing in time. We do it by describing the behavior of an ensemble of proteins characterized by a distribution function $P(X;t)$. The dynamic behavior of X is assumed to be diffusive and therefore the equation for $P(X;t)$ looks as follows:

$$\frac{\partial P}{\partial t} = D\frac{\partial^2 P}{\partial X^2} + \frac{D}{k_BT}\frac{\partial}{\partial X}\left(P\frac{dV}{dX}\right) - k(X)P \qquad (5)$$

where D is the diffusion coefficient and $k(X)$ is the rate constant specified in equation (1). The diffusion motion can itself be characterized as random walk on the energy profile $V(X)$, i.e. it can be viewed as a sequence of random transitions between neighboring conformations. The transition time, τ, between the neighboring conformations is related to the diffusion coefficient as

$$\tau = \frac{k_BT}{D} \qquad (6)$$

This time can also be called "relaxation time" of coordinate X, which characterizes the structural relaxation response of the protein medium to a sudden perturbation, as in the experiments on time-resolved optical spectra (e.g. eosin attached to hemoglobin [21]), as well as in investigations of dynamics of myoglobin [19] and bacterial reaction centers [20] by Mössbauer spectroscopy. Instead of diffusion coefficient D, it is more convenient to deal with this relaxation time parameter τ, which will be the focus of the subsequent discussion.

The initial distribution of X at $t = 0$ is assumed to be thermal,

$$P(X;0) = \frac{1}{\sqrt{2\pi k_BT}}\exp\left(-\frac{X^2}{2k_BT}\right) \qquad (7)$$

In the analysis, the kinetic equation for P is solved numerically and the kinetics of the ET process is described as follows.

The quantity measured in experiment is the survival probability,

$$Q(t) = \int_{-\infty}^{\infty} P(X;t)dX, \quad Q(0) = 1 \qquad (8)$$

The important characteristic of this function is its time derivative at $t = 0$. Using equations (5) and (8), it is easy to show that

$$k_1 \equiv -\dot{Q}(0) = \int_{-\infty}^{\infty} k(X)P(X;0)dX \qquad (9)$$

This quantity is independent of the relaxation time at all temperatures and is, therefore, a characteristic of the equilibrium system. Moreover, it coincides with the rate constant k_e in the slow reaction limit (in the notation and terminology of Sumi and Marcus [13]), or equivalently in the fast diffusion limit ($\tau = 0$), where the decay is single exponential,

$$Q_{fd}(t) = \exp(-k_1t) \qquad (10)$$

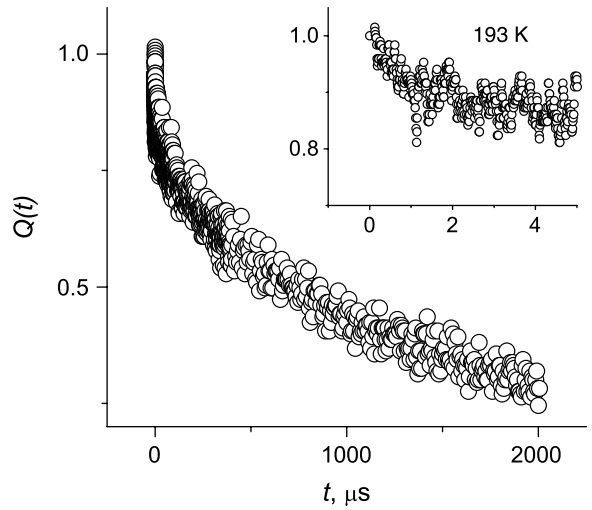

Figure 2. Experimental record at 193 K, long time interval. Inset, the same record, short time interval.

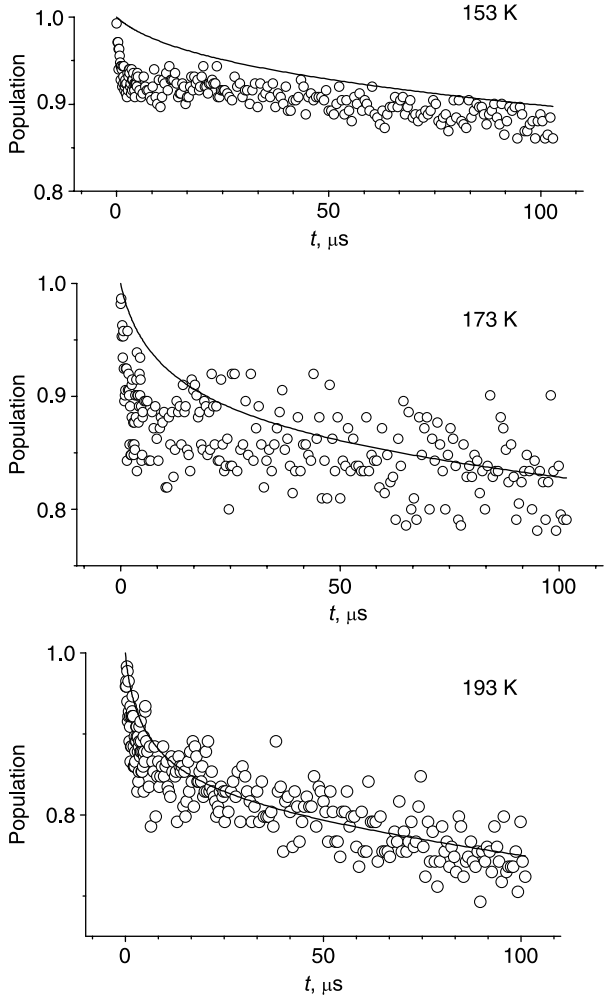

Figure 3. Comparison of the calculated kinetic curves (lines) for Set IV of table 1 and the experimental records (circles) at 153, 173 and 193 K in the non-diffusing limit ($\tau = \infty$).

In the opposite, non-diffusing limit ($\tau = \infty$) the decay is multi-exponential [13],

$$Q_{\mathrm{nd}}(t) = \int_{-\infty}^{\infty} P(X;t)\, \mathrm{e}^{-k(X)t}\, \mathrm{d}X \tag{11}$$

with the same initial rate constant k_1 as $Q_{\mathrm{fd}}(t)$. At any finite relaxation time, $0 < \tau < \infty$, the survival probability initially decays with the same rate constant k_1 and then the decay slows down so that $Q(t)$ falls between $Q_{\mathrm{nd}}(t)$ and $Q_{\mathrm{fd}}(t)$. This is illustrated in figure 1, where curve 1 is $Q_{\mathrm{nd}}(t)$ and curve 4 is $Q_{\mathrm{fd}}(t)$, whereas curves *2* and *3* correspond to intermediate relaxation times.

The strategy for the analysis then is to compare the kinetic curves for Q observed in experiment with the theoretical ones and try to extract information about the dynamics of X, which is basically reduced to finding the relaxation time characterizing the dynamics of X.

Our model contains six generic parameters characterizing the equilibrium state of the system,

$$H_{\mathrm{DA}}, \Delta G^0, \omega_{\mathrm{q}}, \lambda_{\mathrm{q}}, \lambda_{\mathrm{cl}}, \lambda_X \tag{12}$$

They are assumed to be independent of temperature. In addition, we have an unknown relaxation time τ, which is a steep function of T. Thus, overall we have six temperature-independent parameters plus a function of temperature to determine. It is of course impossible to extract all parameters unambiguously unless a wealth of data is available. We will see in the next section how this seemingly dubious task can nevertheless be accomplished. Some details of the fitting procedure, which itself is not a trivial matter are described in Appendix A.

We now go directly to the analysis of experimental data with the theory outlined above.

3. Analysis of experimental kinetic curves

The kinetics of the ET reaction from the proximal heme (c-559) of tetraheme cytochrome to the oxidized primary electron donor, the bacteriochlorophyll dimer (P^+), was measured at 12 temperatures between 193 and 295 K. *Rps. viridis* was grown and reaction centers were prepared as described in Ref. [33]. Purified reaction centers were handled as described in Refs. [34,35]. Flash-induced absorption changes were measured in the time domain of 0.1–2000 μs using a ruby laser as a source of excitation light. The oxidation of the primary donor P and its subsequent reduction were measured by following the 1283 nm absorption of P^+. The cuvette contained 60 vol.% of glycerol. The redox conditions were such that hemes c-559 and c-556 were reduced whereas other hemes oxidized before the flash. The data were published in part in Refs. [36,37]. The interheme ET c-556–c-559 is disregarded in the present analysis since its rate is ten times slower than c-559 to P^+ at all temperatures and the amplitude is only a few percent at $T \geq 200$ K [34–37].

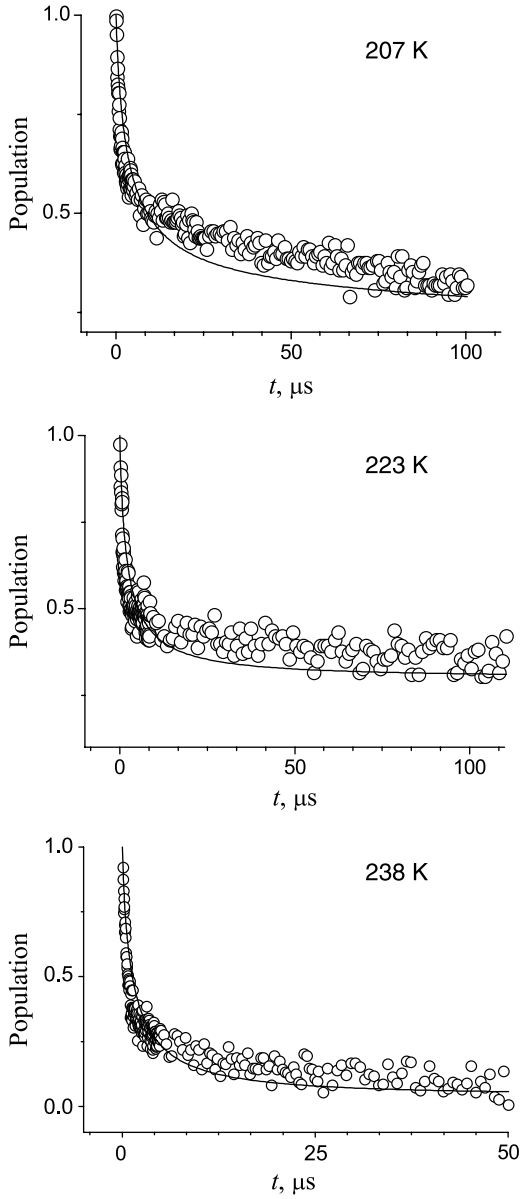

Figure 4. Same as in figure 3 at 207, 223 and 238 K.

The observed kinetics is in fact due to two electron transfer reactions: fast ET from heme c-559 to dimer P^+ and slow ET from quinone Q_A^- to P^+. The scheme of the reaction is the following:

$$\text{c-559} \xrightarrow{\text{fast}} P^+ \xleftarrow{\text{slow}} Q_A^-$$

Scheme 1.

The observed curves include a short-lived component with a rate $\sim 10^6\,s^{-1}$ and a long-lived component with a rate $\sim 10^2\,s^{-1}$. This is demonstrated in figure 2 for 193 K, where the slow kinetics manifests at long times $\sim 2000\,\mu s$ and the fast kinetics is seen at short times $\sim 2\,\mu s$. As described in literature [5,38], the slow component whose rate is practically independent of temperature, is due to the

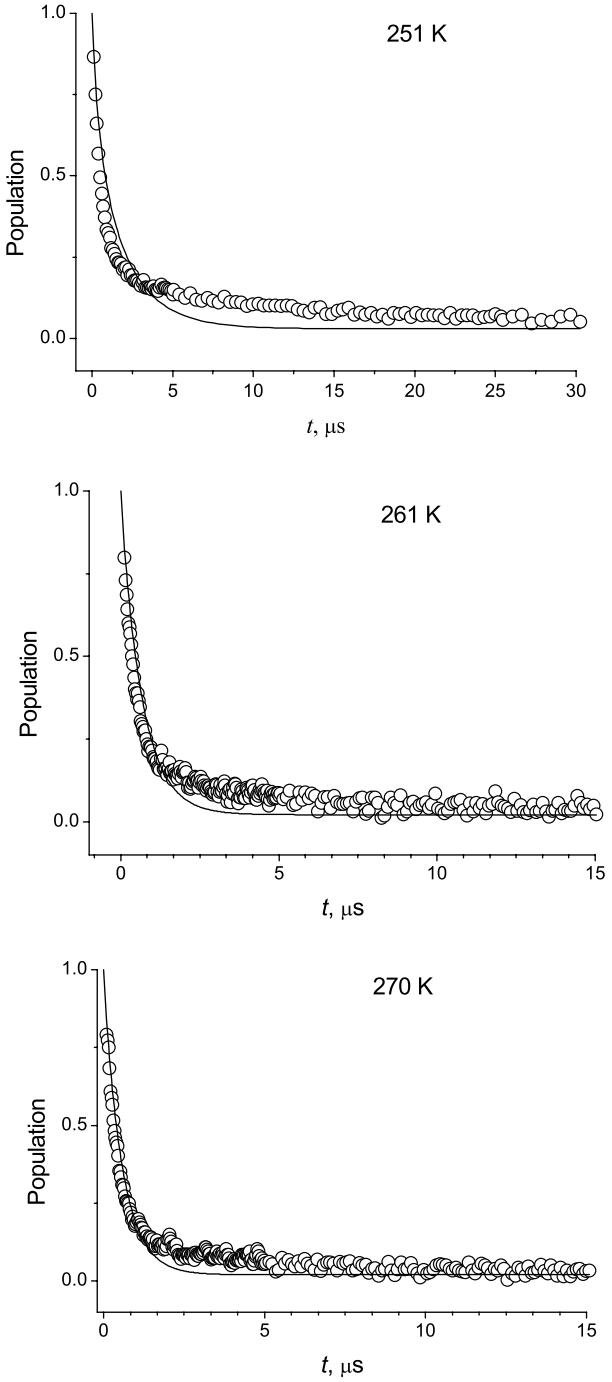

Figure 5. Comparison of the calculated kinetic curves (lines) for Set IV of table 1 and the experimental records (circles) at 251, 261 and 270 K. The quality of the fits is nearly the same for the ranges of τ given in table 2.

ET from the reduced quinone Q_A^- to the oxidized dimer P^+. We are interested in the fast reaction, i.e. the ET from heme c-559 to P^+; this reaction is complete on the time-scale of $\leq 10\,\mu s$. The kinetic curves measured at other temperatures are shown in figures 3–6 by open circles, whereas full lines are calculations by our theory. In the next sub-section, we will describe how the contribution of the slow reaction was eliminated and how the parameters of the model were determined to draw the theoretical curves.

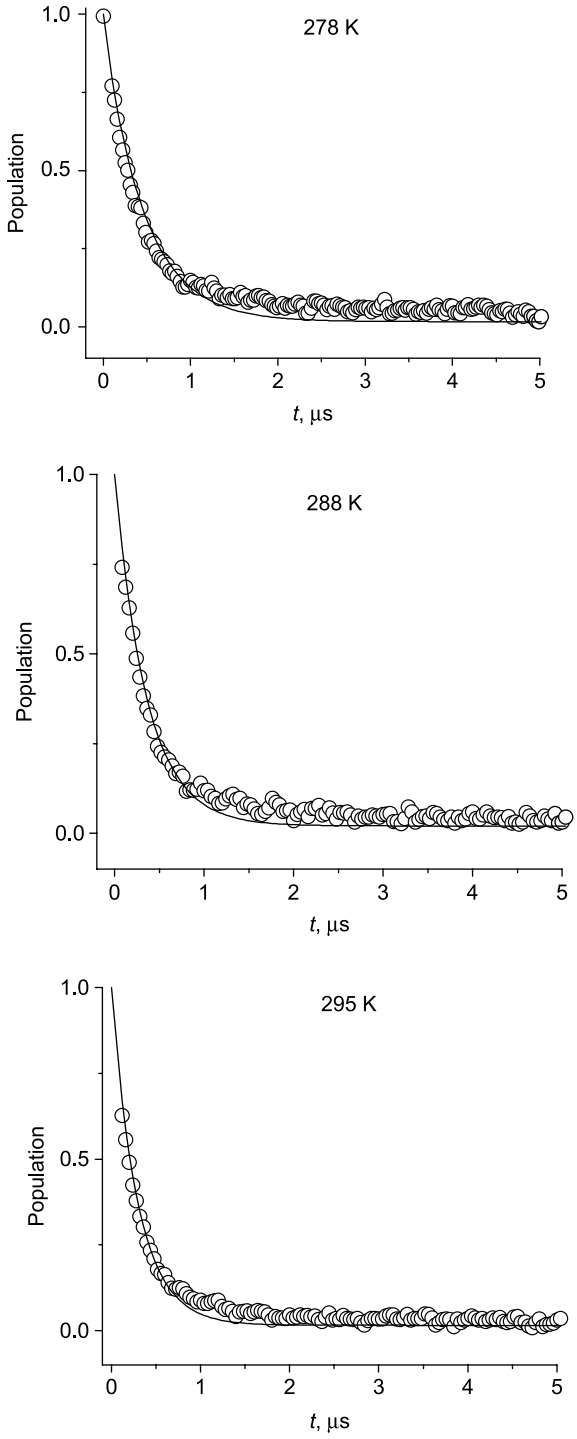

Figure 6. Same as in figure 5 at 278, 288 and 295 K.

3.1 *Elimination of* Q_A^- *to* P^+ *reaction from experimental kinetic data*

An important feature of the fast reaction (c-559 to the dimer) is that it does not go to completion below room temperature, i.e. an appreciable fraction of dimer P^+ remain oxidized on the time-scale as long as 100 μs and longer, while c-559 reduced. At yet longer times, the dimer will be reduced due to a slower reaction of ET from Q_A^- to the dimer (see scheme 1 of the reaction). The fraction of RC's in which the dimer P^+ gets reduced by an electron from c-559 depends on temperature—it *decreases* with decrease of temperature. Therefore, the fraction where the slow ET from Q_A^- to the dimer occurs, *increases* with lowering temperature.

The reason for the fractional nature of ET from c-559 to the dimer at low-temperatures is not entirely clear and is not important for the present study‡. We are interested in the kinetics of those RC's that do react. We, therefore, will subtract the slow kinetic component that is due to ET from Q_A^- to the dimer.

Thus, as the first step in the data processing, we have to separate the contributions of the fast (ET c-559 to P^+) and slow (ET Q_A^- to P^+) protein populations. We will assume that the fast population fully disappears before the reaction in the slow population starts. Then, a moment t_{min} can be defined, such that the amplitudes and rate constants of the slow decay components can be defined from the experimental curves at $t > t_{min}$. We take $t_{min} = 100\,\mu s$ and approximate the slow decay with two exponentials,

$$Q_s(t) = A_{s1}\exp(-k_{s1}t) + A_{s2}\exp(-k_{s2}t) \qquad (13)$$

where the amplitudes and rate constants are variable parameters in a non-linear fitting to the experimental curve $Q_{exp}(t)$. The values of $(1-3)\times 10^2\ s^{-1}$ were obtained for k_{s1} and k_{s2} for all temperatures in accordance with the literature data [5,38]. The sum of the amplitudes, $A_s = A_{s1} + A_{s2}$, is proportional to the number of the reaction centers in the slow population. In the subsequent calculations, we will use A_s, k_{s1}, and k_{s2} to remove the contribution of the slow component, see equation (14) below.

The decay of the fast population at $t < t_{min}$ is also approximated by a bi-exponential expression,

$$\begin{aligned} Q_f(t) &\equiv Q_{exp}(t) - Q_s(t) \\ &= A_{f1}\exp(-k_{f1}t) + A_{f2}\exp(-k_{f2}t) \end{aligned} \qquad (14)$$

Similarly, $A_f = A_{f1} + A_{f2}$ is proportional to the number of the reaction centers in the fast population. We will divide $Q_{exp}(t)$, $Q_f(t)$ and $Q_s(t)$ by the total amplitude, $A_f + A_s$, so that the new amplitudes (for which we retain the same notations) obey the normalization condition $A_f + A_s = 1$. The individual amplitudes and rates of equation (14) are characteristics of the experimental decays and will be used for determination of the model parameters.

‡One possible reason for the fractional nature of electron transfer from c-559 to P^+ is that a protolitic group in a vicinity of the heme of c-559 gets protonated, thereby increasing the potential of the heme. However, the fact that the reaction is practically arrested can hardly be explained in terms of a change in the driving force. An alternative possibility is that the protonation of a group affects the local dynamics of the protein—say, hindering reorientations of water dipoles, which can significantly affect the rate. For instance, if the extra proton present in the slow population forms an H-bond between an amino acid residue and/or a water molecule in the interior of the protein, then reorientation of a particular dipole may become prohibited, which in its turn can fully stop the reaction

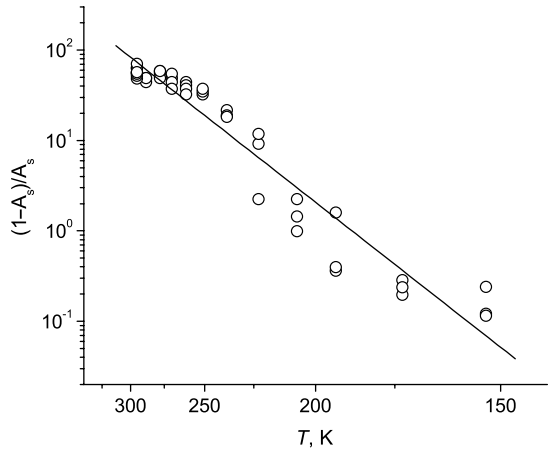

Figure 7. Plot of $\log[(1 - A_s)/A_s]$ vs. $1/T$. Circles, experimental data; line, equation (15) with $\Delta S = 1.0\,\mathrm{meV/K}$ and $\Delta E = 0.19\,\mathrm{eV}$.

The temperature dependence of A_s can be represented by the equation

$$A_s = \left[1 + \exp\left(\frac{T\Delta S - \Delta E}{k_B T}\right)\right]^{-1} \tag{15}$$

where ΔS and ΔE stand for the changes in entropy and energy between the deprotonated and protonated states. In figure 7, the ratio $(1 - A_s)/A_s$ is plotted as a function of temperature. From a linear least-squares fit, the values of $\Delta S = +11.8 \times k_B = 1.0\,\mathrm{meV/K}$ and $\Delta E = +0.19\,\mathrm{eV}$ are obtained.

The positive signs mean that the entropy and energy are higher in the state in which the fast reaction (c-559 to P^+) is not arrested. If we assume that the arrest is due to protonation of a group near heme of c-559, the pK_a of this group can be calculated from the above values of ΔS and ΔE as

$$pK_a = \mathrm{pH} - \frac{T\Delta S - \Delta E}{k_B T \ln(10)} \approx 6$$

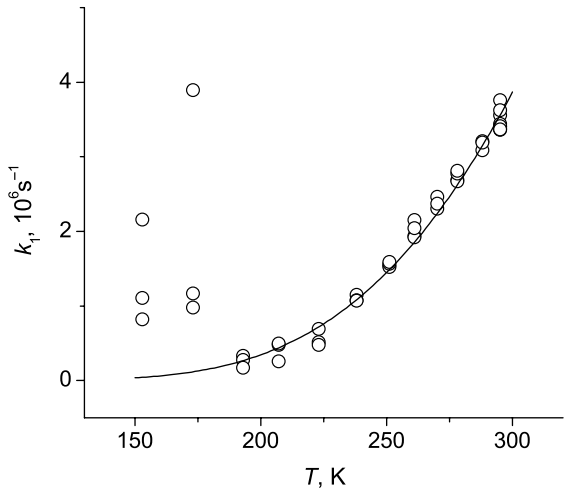

Figure 8. Plot of k_1 vs. T. Circles, experimental data; line, theoretical curve, equation (20) with parameters from table 1.

Table 1. The parameters of the model, Set IV (see Appendix A.4).

Generic parameters
$H_{DA} = 2.2\,\mathrm{cm^{-1}}$
$\Delta G^0 = -1100\,\mathrm{cm^{-1}}$
$\hbar\omega_q = 800\,\mathrm{cm^{-1}}$
$\lambda_q = 284\,\mathrm{cm^{-1}}$
$\lambda_X = 718\,\mathrm{cm^{-1}}$
$\lambda_{cl} = 6175\,\mathrm{cm^{-1}}$
Basic parameters
$k_0 = 4.7 \times 10^9\,\mathrm{s^{-1}}$
$p = 7.81$
$p_{cl} = 7$
$x_m = 9.02$
$k_1(193) = 0.261 \times 10^6\,\mathrm{s^{-1}}$
$k_1(295) = 3.48 \times 10^6\,\mathrm{s^{-1}}$
$k_2(193) = 0.3 \times 10^6\,\mathrm{s^{-1}}$

at $T = 295\,\mathrm{K}$ and pH 8. At room temperature, this group is fully deprotonated, while at low-temperatures, it gets a proton which presumably affects the fast reaction. One needs to remember however, that the true nature of incompleteness of the c559 to P^+ reaction is not known.

After elimination of the contribution from the slow Q_A^- to P^+ reaction, equation (14), we can focus entirely on the reaction of our interest, ET c-559 to P^+ and determine the model parameters for this reaction according to our theory.

3.2 Determining basic parameters of the model

As shown in Appendix A.1, only four basic static parameters define the equilibrium properties of the system in our model,

$$k_0, x_m, p_X, p_{cl} \tag{16}$$

which are some combinations of the original parameters, equation (12). The basic parameters are to be found from experiment with a restriction that the resulting generic parameters can be assigned "reasonable" values, which do not contradict to the available data and the common sense.

Obviously, the initial six parameters in equation (12) cannot be uniquely defined given only four parameters in equation (16). We fix two of them at the following values:

$$\Delta G^0 = -1100\,\mathrm{cm^{-1}}, \quad \hbar\omega_q = 800\,\mathrm{cm^{-1}} \tag{17}$$

The value of ΔG^0 was estimated by Frolov *et al.* [20]. The quantum frequency is typical for intra-molecular vibrations. Variations of ω_q while keeping parameters in equation (16) constant result in redefinitions of the reorganization energies.

To define four equilibrium parameters, we use the experimental values of k_1, which are independent of τ. In the next section and Appendix A.2, we describe how these parameters were actually obtained from the experimental data. The best set of parameters is given in table 1.

The general strategy of our analysis is to determine first the static parameters, equation (16), from the low- and high-temperature data; after that, the dynamical parameter τ can be found from the intermediate-temperature data.

Table 2. The relaxation time, τ and the corresponding error bar, $\Delta\tau$, calculated for each experimental record.

Record	*T (K)*	*τ (μs)*	*Δτ (μs)*
02	295	0.018	0.009–0.029
04	295	0.059	0.026–0.11
05	295	0.033	0.023–0.044
06	295	0.064	0.029–0.12
07	295	0.045	0.027–0.068
08	295	0.053	0.038–0.071
09	295	0.057	0.024–0.095
10	295	0.054	0.029–0.086
11	295	0.020	0.0069–0.037
14	261	0.090	0.048–0.15
15	261	0.47	0.24–0.87
16	261	0.80	0.50–1.23
17	261	0.19	0.10–0.32
18	251	1.1	0.66–1.8
19	251	1.7	1.25–2.3
21	251	1.79	0.45–1.35
22	251	0.75	0.42–1.3
23	270	0.13	0.092–0.19
24	270	0.12	0.054–0.21
25	270	0.074	0.055–0.095
26	270	0.077	0.041–0.13
27	278	0.055	0.038–0.073
28	278	0.055	0.039–0.074
29	278	0.049	0.019–0.088
30	278	0.039	0.010–0.079
31	288	0.039	0.024–0.057
33	288	0.053	0.032–0.077
34	288	0.038	0.013–0.070

The function $\tau(T)$ is found by solving the diffusion-reaction equation, equation (5), at various values of τ, so that τ at a given T is obtained from the best fit to experiment. The $\tau(T)$ obtained in this way is fitted by the function

$$\tau(T) = \tau_\infty \exp\left(\frac{E_a}{k_B T}\right) \tag{18}$$

where E_a is the activation energy and τ_∞ the pre-factor.

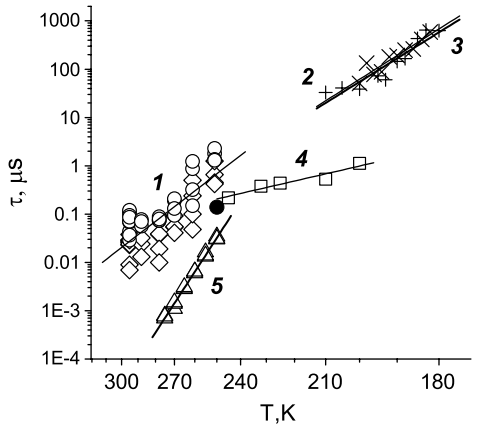

Figure 9. The calculated and measured relaxation time for various systems as a function of temperature (logarithm of time vs. reciprocal of temperature). Circles and rhombs, the upper and lower bounds on τ, respectively, calculated in this paper (data from table 2). Line ***1***, the least squares fit giving $E_a = 0.45$ eV, $\tau_\infty = 5{\cdot}10^{-16}$ s. Plusses and crosses, the optical spectroscopy data [22] on the dielectric relaxation of a glycerol–water solution (60 vol.% of glycerol) and of hemoglobin in the same solution, respectively (see Section 4). Lines ***2*** and ***3***, the least-squares fits giving similar values of $E_a = 0.37$ eV, $\tau_\infty = 3 \times 10^{-14}$ s. Squares and triangles, the data of Mössbauer spectroscopy on heme iron in myoglobin [20] and on free iron ion in a glycerol–water mixture (94 vol.% of glycerol)[42], respectively. Lines ***4*** and ***5***, the least squares fits giving $E_a = 0.14$ eV, $\tau_\infty = 4 \times 10^{-10}$ s and $E_a = 0.91$ eV, $\tau_\infty = 2 \times 10^{-26}$ s, respectively. Filled circle, estimated by Frolov *et al.* [21] from Mössbauer data on reaction centers from *Rps. viridis*. For comments on the experimental data, see Sections 4 and 5.

3.3 *Fitting the kinetic curves and determining* $\tau(T)$

We first focus on the initial decay of the fast population, characterized by k_1. This rate is a useful characteristic because it is independent of the dynamical variable τ at all temperatures and therefore it helps to determine the static (i.e. independent of τ) parameters of the model, equation (12). The experimental values of k_1 were calculated by the first part of equation (9), where $Q(t)$ is replaced with $Q_f(t)$ from equation (14), to give

$$k_{1\exp} = A_{f1}k_{f1} + A_{f2}k_{f2} \tag{19}$$

The data are shown in figure 8. Three to four measurements were performed at each temperature (9s at 295 K). The measured curves are well reproducible above the glass transition temperature (data at $T \geq 193$ K) and the values of k_1 calculated by equation (19) smoothly increase with increasing temperature, showing a small scatter. Unfortunately, at 153 and 173 K, the kinetic curves are very different between successive measurements, which manifests as a large scatter in the k_1 values. Therefore, we will rely on the data at $T \geq 193$ K. The theoretical values were calculated by equation

$$k_1 = \frac{k_0}{\sqrt{1 + p(T/T_g)}} \exp\left[-\frac{x_m^2}{1 + p(T/T_g)}\right] \tag{20}$$

which follows from equations (28) and (29) of Appendix A.1. In figure 8, the theoretical curve $k_1(T)$ calculated with the use of the parameters from table 1 is shown. The selection of the static parameters is described in the next section and Appendix A.2. A good agreement in the entire temperature interval from 193 to 295 K assures that the theoretical kinetic curves will follow the experimental ones at least at the initial stage of decay.

Given the equilibrium parameters of table 1, we calculate the theoretical curve, $Q_{theor}(t)$, at a given T and various values of the relaxation time τ. The theoretical curve is calculated as the sum of the contributions from the fast and slow populations,

$$Q_{theor}(t) = A_f Q(t) + Q_s(t) \tag{21}$$

where A_f and $Q_s(t)$ were defined as described in Section 3.2. The function $Q(t)$ describing the decay of the fast population is found as follows: at a given temperature, we solve the diffusion-reaction equation, equation (5), for various values of τ by expansion in the harmonic basis set [39,40] (see Appendix B) and find τ that gives the best agreement with the experimental curve.

In the range of temperatures $251 \leq T \leq 295$ K, τ could be determined by the procedure described above. Of course, the fitting procedure is not unambiguous and

for each set of the experimental data, the best value of τ is determined with a corresponding error bar, $\Delta\tau$. Table 2 gives the results of the data analysis and shows typical ranges of obtained in the fitting procedure.

The data are also depicted in figure 9 where the lower and upper bounds on τ are plotted versus inverse temperature. They are fitted by equation (18). The result for τ in terms of the activation energy and the pre-exponential factor is $E_a = 0.45\,\text{eV}$ and $\tau_\infty = 5 \times 10^{-16}\,\text{s}$, respectively. Several tests were performed in Appendix A.3 in order to check the stability of the results. Other sets of parameters are treated in Appendix A.4. Collecting all data, we obtain that the activation energy for the dipole reorientation in the protein matrix lies in the interval of 0.4–0.6 eV, which is the main result of the present work.

At temperatures below 251 K, the experimental data were collected at $T = 238$, 223, 207, 193, 173 and 153 K. For such temperatures, the fitting procedure with varying τ becomes very inaccurate. For 193 K, for example, the only estimate one can obtain from the fitting is that the relaxation time $\tau > 10\,\mu\text{s}$. The reason for such a problem is that the time-scale of ET, which is less than 2 μs, becomes shorter than that of relaxation of the medium; at such conditions, the rate of the observed reaction is no longer sensitive to the actual dynamics of the medium and the medium can be considered as "frozen" on the time-scale of the reaction. The kinetics of the ET reaction in such a case is determined by equation (11).

The large relaxation time determined from the experimental data is consistent with the temperature dependence of τ determined for 251–295 K, which predicts that the relaxation time should be 2 μs at 238 K and 300 μs at 193 K. The increase of the relaxation time is in fact even more dramatic when the glass transition temperature ($T_g \approx 180\,\text{K}$) is approached. Thus, at temperatures below roughly 200 K, the protein medium should be considered as static, as far as our ET reaction is concerned. The relaxation parameters E_a and τ_∞ found for temperatures 251–295 K are probably also good down to say 238 K, but not much lower, because of the closeness of the glass transition at 180 K.

Figures 3–6 show the comparison of the experimental kinetic curves with theoretical predictions for the parameters determined as described above. In figures 3 and 4, the kinetic curves are shown for T in the range 153–238 K. At these temperatures, the determined relaxation time τ is so large (on the time-scale of the reaction) that the reaction is considered to occur in a "frozen" medium and the rate is calculated by equation (11).

For very low-temperatures, 153 and 173 K, there is significant disagreement between the theory and experiment at the initial stage (a few μs) of the decays. This most likely is related to the glass transition, which affects all dynamics of the protein, not only our coordinate X. Above the glass transition temperature, already at 193 K, figure 3 and higher temperatures, figure 4, the comparison of experiment and theory is much better. Figure 4 still describes the low-temperature frozen-medium limit of the theory.

Figures 5 and 6 refer to temperatures in the range of 251–295 K. This is the dynamically controlled ET regime *per se*, i.e. each curve depends on the relaxation time τ (not shown in the figures, see below). As seen from table 2, there is a quite large scatter of the τ values at each temperature. This means that the quality of the fits in figures 5 and 6 does not vary appreciably when τ varies within the intervals shown in table 2. Because of such a low sensitivity of the method, the individual values of τ make little sense and only the general trend derived from the statistical analysis in figure 9 is significant. It should be remembered that all 12 curves shown in figures 3–6 are described with the same set of static parameters. The agreement with experiment is quite good, as one can see.

Summarizing, our theory is able to describe a wealth of experimental kinetic data with a limited set of physical parameters; the procedure is such that the most interesting dynamic parameter τ and the corresponding E_a and τ_∞ of equation (18) could be determined with a reasonable degree of accuracy.

4. Comparison with other methods

Since our goal here is to extract the relaxation time of a protein immersed into a glycerol–water mixture, it is of interest to mention other methods to monitor relaxations of proteins and super-cooled liquids. Kotelnikov *et al.* [21] developed a method based on measuring the time-resolved shift of the maximum of the phosphorescence spectrum, $\nu(t)$, of the xanthene dye eosin dissolved in a glycerol–water solution (60 vol.% of glycerol) at various temperatures. In a different experiment, eosinisothiocyanate was covalently bound to the SH group at the surface of hemoglobin immersed into the same solution. At $T < 170\,\text{K}$, where the medium was frozen, the maximum of the spectrum did not change in time, $\nu = \nu_0$. At higher temperatures, above the glass transition point, a decrease of ν from ν_0 at $t = 0$ down to $\nu_\infty < \nu_0$ at long times was observed due to dielectric relaxation of the medium. The lifetime of the excited triplet level of eosin at $T = 90 - 170\,\text{K}$ is 0.67 ms, which enabled measuring the dielectric relaxation times in the range of $1 - 10^4$ μs. The use of fluorescent probes [24] will permit monitoring the protein dynamics on the nanosecond time scale.

The results of these experiments are shown in figure 9, data sets **2** and **3** for the triplet probe either dissolved in the solution or attached to the surface of hemoglobin, respectively. Obviously, the relaxations of the solution were monitored in both cases, with only a small contribution from the protein in the latter case. When comparing with our data on the bacterial reaction centers, data set **1**, we note that, first, the reaction centers were immersed into a solution of nearly the same composition as in **2** and **3** and second, the influence of the protein dynamics should be more pronounced than in **3** since ET

occurs between the redox centers buried inside the protein body. The similar activation energies obtained in both cases imply that the relaxation of the solution plays a major role. A slightly higher activation energy and a wider data scatter for the reaction centers might be due to the protein contribution and in particular, the result of a broad distribution of the protein relaxation times [2,3,19], which was not accounted for in the present treatment.

Chang *et al.* [19] and Nienhaus *et al.* [41] used Mössbauer spectroscopy on iron to measure relaxations in myoglobin and glycerol, data sets **4** and **5**, respectively. In the Mössbauer experiments, a different kind of dynamics is monitored associated with the random motion of the iron ion. Yet, as demonstrated by Nienhaus *et al.* [41], the motion of the Mössbauer nuclei is closely coupled to the structural relaxation, giving an average relaxation time similar to the times of dielectric and ultrasonic volume relaxations. A drastic difference in relaxation between myoglobin crystal, data set **4** and nearly pure glycerol, data set **5**, is noticeable. The existence of conformational substates in proteins makes structural rearrangements easier to perform, thereby decreasing the activation energy and may also result in an increased broadening of the relaxation times distribution with increasing temperature [19]. Both these features are definitely of importance for electron transfer under study. Unfortunately, the relaxation time distribution cannot be taken into account in frames of the present approach because the procedure would become too complicated.

Frolov *et al.* [20] measured the temperature dependence of the mean-square displacement of iron atoms in reaction centers from *Rps. viridis* by Mössbauer spectroscopy. They found it to steeply increase with temperature increasing from 200 to 300 K and reached the half-maximum value at 250 K, which corresponds to the protein relaxation time approximately equal to the lifetime of the excited nuclear level, 0.14 μs. This single point is shown in figure 9 by the filled circle, which falls within the data set **1** obtained in this paper.

5. Discussion

We have described an example of how ET reaction in a protein can be used as a probe of protein dynamics. This method provides insights into dynamic characteristics of the protein on a time-scale of few microseconds and is complementary to other methods in this area, regarding the specific temperature and time intervals, as demonstrated in Section 4 by comparison with the experimental results by optical and Mössbauer spectroscopy.

A limitation on the method is imposed by the fact that the kinetics of the ET is insensitive to the medium dynamics when the ET rate is either too fast or too slow compared to the dynamics time-scale τ of the protein. In this respect, the ET from c-559 to P^+ in bacterial reaction centers provides an example where in the range of temperatures from the glass transition to room temperature, there is a window of temperatures at which the relaxation time of the protein medium is comparable to the ET time-scale, which results in sensitivity of the ET kinetics to protein dynamics utilized in this work.

In our model, the structural protein dynamics (i.e. the slow component of the dynamics of the protein coupled to the ET process) is represented by a generalized coordinate X, which is characterized by the relaxation time $\tau(T)$. The relaxation time is a sensitive function of temperature T and has a typical activation form, equation (18), with parameters E_a and τ_∞, which we determined from the analysis of the kinetics of the ET reaction at different temperatures. Our results show that it is 0.5 ± 0.1 eV and τ_∞ is within 10^{-15}–10^{-17} s. The determined pre-factor τ_∞ is much too small for a system that could be described by a simple transition state theory, however, not unusual for such relaxation characteristics of viscose media as supercooled glycerol–water solutions [42] (see also a comment in Ref. [5] below). The activation barrier can correspond, for example, to breaking of H-bonds in the dynamics of X, however, the phenomenological nature of the model does not allow more specific conclusions at this stage.

The model that we apply for the analysis is similar to that of Sumi and Marcus [13], yet not identical to it. In their theory, only two generalized modes—a non-diffusive mode q and a diffusive mode X—were used. We find that the original two-mode model does not work: we were unable to fit the experimental curves with the parameters for one mode q and one slowly relaxing medium mode X. Instead, we find that it is absolutely necessary to include non-diffusive classical modes of the medium, which provide the largest contribution to the total reorganization energy, as seen from table 1.

The kinetics of ET from c-559 to P^+ has revealed an unexpected feature: at low-temperatures the reaction proceeds in such a way that only in a fraction of proteins the P^+ is reduced by the electron from c-559 on the time-scale of a few μs. In the rest of proteins, this reaction appears to be arrested (at least on the time-scale of 100 μs) and the reduction of P^+ occurs by the electron from Q_A^-. This prompted us to introduce two populations (two ensembles) of the proteins—fast (ET c-559 to P^+) and slow (ET Q_A^- to P^+), as shown in scheme 1. The nature of the factors that result in such an arrest of the reaction from c-559 is not clear at present, however, the analysis of the temperature dependence of the fraction of protein reacting (fast population) indicates that it could be a protonatable group with $pK_a \approx 6$ at $T = 295$ K that is protonated in the slow population at low-temperatures, thereby somehow slowing down the reaction.

In our model, the multi-exponential decay of the fast population is caused by a *static* heterogeneity, which is described by the dependence of the rate constant upon the X coordinate. Previously, we proposed a model where *dynamic* heterogeneity, i.e. a distribution of the relaxation times, was supposed to be responsible for the multi-exponential kinetics of a similar reaction in *Rhodopseudomonas sulfoviridis* [1–3]. The Cole–Davidson

Table 3. The activation energy and the pre-exponential factor of $\tau(T)$, equation (18).

Test	E_a *(eV)*	τ_∞ 10^{-15} *(s)*	*Notes*
1	0.45	0.5	Determined by $\Delta\tau$ from table 2[†]
2–8	0.54	0.01	Determined by $\Delta\tau$ from table 2[‡]
9	0.44	0.9	Determined by τ from table 2[†]
10–12	0.52	0.03	Determined by τ from table 2[‡]
13	0.49	0.1	Determined by $\Delta\tau$, STD100, ΔSTD = 0.002[¶]
14–16	0.52	0.03	Determined by $\Delta\tau$, STD100, ΔSTD = 0.002[‡]
17	0.43	1.2	Determined by $\Delta\tau$, STD5, ΔSTD = 0.001[†]
18–20	0.51	0.03	Determined by $\Delta\tau$, STD5, ΔSTD = 0.001[‡]
21	0.44	0.7	Determined by $\Delta\tau$, STD5, ΔSTD = 0.002[§]
22–24	0.51	0.04	Determined by $\Delta\tau$, STD5, ΔSTD = 0.001[‡]
25	0.42	2.1	Determined by τ, STD[†]
26–28	0.50	0.07	Determined by τ, STD[‡]
Summary: $E_a = 0.42–0.54$ eV, $\tau_\infty = (0.01–2.1) \times 10^{-15}$ s			

[†] All records.
[‡] Five records at 295 K are omitted. For a given set of tests, only the one with the maximum deviation from the result of Test I is shown, see text.
[¶] All records except 02, 11 and 30, for which the lower bound on τ could not be defined.
[§] All records except 02, for which the lower bound on τ could not be defined.

distribution was used to represent the dynamic heterogeneity, as is common for studies of relaxation. It was obtained that the characteristic parameter β of the Cole–Davidson distribution decreased with increasing temperature. The same trend was observed in Ref. [19] for myoglobin crystal.

Our X coordinate, which describes conformational dynamics of the protein, is virtually equivalent to the ε coordinate in the model proposed by McMahon *et al.* [5] in their studies of the slow reverse ET from Q_A^- to P^+ at cryogenic temperatures. These authors introduced a distribution of energy gaps between the donor and acceptor states to account for the structural (conformational) heterogeneity in the sample. They discussed four different types of conformational states with dynamics on the time-scale from 0.1 to 10^4 s, with the corresponding activation energies 0.2–1 eV and prefactors 10^{-13}–10^{-25} s.

Gray *et al.* [6–10] investigated large-scale conformational changes of proteins using electron and energy transfer as a probe. Transitions between folded and unfolded conformations typically occur on the time scales of 1 ms–1 s [7,9–10]. Faster conformational changes, on microsecond [6] and submicrosecond [8] time-scales, could be observed as well. In this paper, we deal only with short-scale conformational changes around the donor and acceptor sites, which influence the driving force of the reaction keeping the electronic coupling constant.

The present measurements were performed at 12 temperatures between 153 and 295 K. No unique set of the four basic parameters could be defined from fitting 12 experimental kinetic curves, therefore, the most interesting parameter of the model, $\tau(T)$, could be also determined only within some error bars. The variations are not very dramatic, however and the result is meaningful, as shown in table 3 of Appendix A.3.

Formally, we deal with a model that contains six static temperature independent parameters and one dynamic temperature dependent parameter, $\tau(T)$. In fact, however, two of the static parameters (ΔG^0 and ω_q, see equation (17)) were fixed at constant values selected from general considerations and one more parameter (p_{cl}, see Appendix A.4) influenced the results very weakly. Six low-temperature curves in figures 3 and 4 were considered as independent of the dynamical variable τ and were fitted only with three static parameters. Fittings of the six high-temperature curves in figures 5 and 6 were performed with the same set of static parameters plus the dynamic parameter τ individually selected for each curve. Therefore, the level of agreement with the kinetic curves at 12 different temperatures is noteworthy.

Acknowledgements

The authors are grateful to M. V. Basilevsky for helpful discussions. This research was supported by the Russian Foundation for Basic Research (05-03-32104), the US Civilian Research and Development Foundation (RUC2-2658-MO-05), and NIH grant GM54052 to AAS.

A Details of the fitting procedure

A.1 Introducing dimensionless parameters

It is convenient to introduce a new variable,

$$y = \frac{X}{\sqrt{2k_B T}} \tag{22}$$

in order to bring equation (5) into a form where the diffusion operator depends only on the relaxation time τ whereas all parameters characterizing the equilibrium state are moved to the reaction rate. The latter is written in terms of the new variable as

$$k(X) = \frac{k_0}{\sqrt{\alpha}}\kappa(y), \quad \kappa(y) = \exp\left[-\frac{(x_m - by)^2}{\alpha}\right] \tag{23}$$

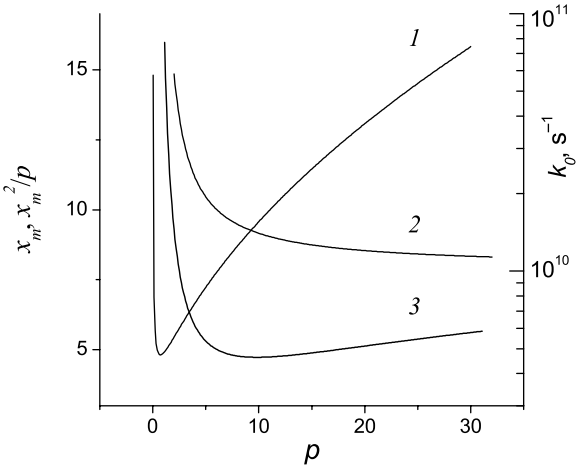

Figure 10. Plots of x_m (curve 1), x_m^2/p (curve 2) and k_0 (curve 3) vs. p.

where

$$k_0 = \frac{H_{DA}^2}{\hbar}\sqrt{\frac{2\pi}{\hbar\omega_q\lambda_q}} \tag{24}$$

$$\alpha = \coth\left(\frac{\hbar\omega_q}{2k_BT}\right) + p_{cl}\frac{T}{T_g}, \quad p_{cl} = \frac{2k_BT_g\lambda_{cl}}{\hbar\omega_q\lambda_q} \tag{25}$$

$$x_m = \frac{\Delta G^0 + \lambda}{\sqrt{2\hbar\omega_q\lambda_q}}, \quad \lambda = \lambda_q + \lambda_{cl} + \lambda_X \tag{26}$$

$$b = \sqrt{p_X\frac{T}{T_g}}, \quad p_X = \frac{2k_BT_g\lambda_X}{\hbar\omega_q\lambda_q} \tag{27}$$

The glass transition temperature, T_g, was artificially introduced into these equations to make the parameters p_{cl} and p_X dimensionless. The rate constant of the initial decay is calculated from equations (1), (7) and (9) to give

$$k_1 = \frac{k_0}{\sqrt{\alpha + b^2}}\exp\left(-\frac{x_m^2}{\alpha + b^2}\right) \tag{28}$$

Replacing the first term of α in equation (25) by unity, we obtain

$$\alpha + b^2 = 1 + p\frac{T}{T_g} \tag{29}$$

where $p = p_{cl} + p_X$ is a new parameter to be used in fitting the experimental data.

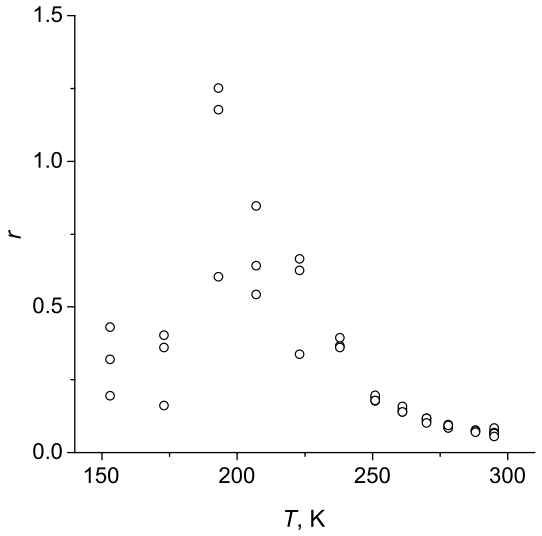

Figure 11. The measure of non-exponentiality of the experimental curves as function of temperature. Zero ordinate corresponds to a single-exponential decay.

A.2 Selection of the parameters

As explained in the main text, the equilibrium parameters are defined from the low- and high-temperature data. In particular, the values of k_1 will be used. The average experimental values at 193 and 295 K are given in table 1. It is seen from equations (28) and (29) that the theoretical ratio $k_1(295)/k_1(193)$ is a function of only two parameters, x_m^2 and p. Equating this ratio with its experimental value, we obtain x_m^2/p and x_m (up to the sign) as functions of p. Further, equating the theoretical expression of $k_1(193)$ with its experimental value, we obtain k_0 as a function of p.

These functions are shown in figure 10. In the low-p region, $p < 5$, curves *2* and *3* rapidly increase, which results in unrealistic values of the generic parameters, equation (12). The sign of x_m can be positive or negative, corresponding to the reaction in the normal and inverted regions, respectively. The generic parameters, equation (12), calculated with negative x_m also take unrealistic values, therefore, $x_m > 0$ will be used. The analysis in Ref. [21] also indicates that the reaction is in the normal region.

Thus, the problem is reduced to a selection of only two equilibrium parameters, p and p_{cl}. There is no unique way to make a right choice. In practice, we used the second derivative of the initial decay. In general, this quantity depends on τ. However, for the initial Boltzmann distribution a simple relation similar to equation (9) can be easily obtained,

$$k_2 \equiv \ddot{Q}(0) = \int_{-\infty}^{\infty} k(X)^2 P(X;0)\,dX \tag{30}$$

which again is independent of τ. The experimental values calculated from equation (14) as

$$k_{2exp} = A_{f1}k_{f1}^2 + A_{f2}k_{f2}^2 \tag{31}$$

are shown in figure 11 in the form of $r = (k_2/k_1^2) - 1$. For single-exponential decay one has $r = 0$, therefore r is a measure of how far the experimental curve declines from a single exponential. Again, a large scatter is seen at 153 and 173 K. The large value of r at 193 K indicates that the decay strongly declines from a single exponential behavior. At increasing temperature, r decreases and the decay is nearly single exponential at room temperature.

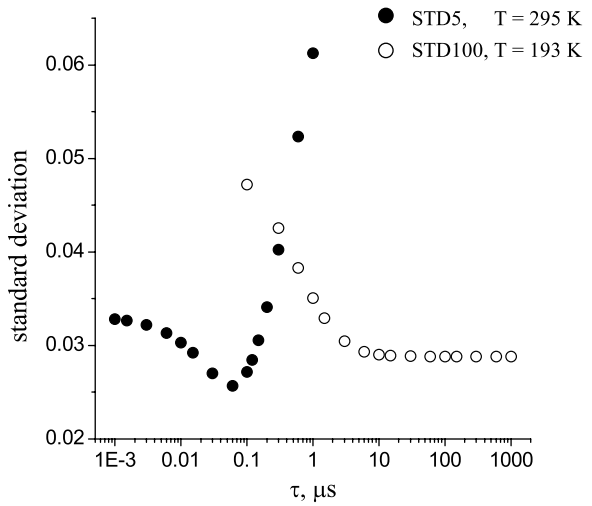

Figure 12. STD of the theoretical curves from the experimental ones as functions of the relaxation time.

Table 4. The parameters of the model, Sets IX–XIII.

Parameter	*Set IX*	*Set X*	*Set XI*	*Set XII*
H_{DA}, cm^{-1}	1.83	1.71	1.66	1.60
λ_q, cm^{-1}	128	73	47	19
λ_X, cm^{-1}	682	669	662	655
λ_{cl}, cm^{-1}	5994	5926	5893	5857
K_0, $10^9\,s^{-1}$	4.9	5.7	6.7	9.9
p	17	29	44	110
p_{cl}	15	26	40	100
x_m	13	16	20	31

Parameters missing in this table are the same as in table 1.

The use of the second derivative is limited because it is defined from experiment with a much lower precision than the first derivative. In addition, the precision is rapidly decreasing with increasing temperature. Therefore, we will use k_2 at 193 K as a variable parameter instead of p. The advantage of k_2 over p is that we have the average experimental value of $k_2(193) = 0.154$ as a reference point. The value 0.3 shown in table 1 gives satisfactory results for the kinetic curves. If we impose the restriction on the theoretical value of k_2 to be equal to the latter, we obtain a connection between p and p_{cl} (not shown). The resulting p is slightly larger than p_{cl}.

Thus, we arrived at the following picture. The restrictions imposed on the values of k_1 at 193 and 295 K decreased the number of the parameters to be adjusted from four to two, namely p and p_{cl}. Using $k_2(193)$ instead of p narrows the range of possible variation. It was observed that the reference value of $k_2(193)$ gave satisfactory results for fitting the low- and high-temperature kinetic curves (with an appropriate choice of p_{cl}), but fittings at intermediate temperatures were poor. Increasing $k_2(193)$ by about two times resulted in a better agreement at intermediate temperatures, but the agreement became worse for the low-temperature data while the high-temperature results remained good. A further increase in $k_2(193)$ confirmed this trend, so that the value shown in table 1 was selected as a compromise.

Further, $p_{cl} = 7$ was selected to start with, which gave p shown in table 1. As was said in the discussion of figure 10, the low values of $p < 5$ lead to unrealistic values of the generic parameters. The same is true of the very large p values. Therefore, the above values of p_{cl} and p seem to be a good starting point for our analysis.

Given the values of four basic parameters in equation (16), the generic parameters in equation (12) were defined as follows. Inserting ΔG^0, x_m and $\hbar\omega_q$ into equation (26), we obtain a quadratic equation with respect to $\sqrt{\lambda_q}$. Then, λ_{cl} and λ_X are defined from equations (25) and (27). The results are collected in table 1.

A.3 Details of determining $\tau(T)$. Testing stability of the results for the activation energy and pre-factor

At a given temperature, we solve the diffusion-reaction equation (5) (see Appendix B) repeatedly for various values of τ in order to reach the best agreement with the experimental curve. As a quantitative measure of the quality of the fit, standard deviations within time intervals of 0–5 or 0–100 μs (STD5 or STD100, respectively) were used. The STD vs. τ curves behave very differently at low- and high-temperatures as demonstrated in figure 12 for two temperatures. At 193 K the standard deviation is independent of τ at $\tau > 10$ μs and increases at $\tau < 10$ μs. While the protein mobility is expected to manifest above the glass transition temperature (≈ 180 K), the relaxation time at 193 K cannot be defined by the present method and only a lower bound on τ can be found. This is also the case for 207, 223 and 238 K. In contrast, at 295 K the STD reaches a minimum, STD_{min}, at a value of τ somewhere between 0.01 and 0.2 μs. Since the minimum is very flat, the values of τ at the minimum are defined poorly. Therefore, we put a "gate" around STD_{min}, ΔSTD and find the upper and lower bounds on τ such that the respective values of STD are $STD_{min} \pm \Delta STD$. The calculated data are collected in table 2, where the first column is the number of the experimental record (the data file), the second column gives the values of τ at the minimum of STD100 and the third column shows the range of τ variation within the STD interval of 0.001 around the minimum. The data are also presented in figure 9, where the lower and upper bounds on τ from table 2 are plotted vs. the inverse temperature. They are fitted by equation (18). The results obtained are shown in the first row of table 3 (test 1).

The calculated values of E_a and τ_∞ depend on the method used. In particular, as shown in table 2, nine experimental records were made at 295 K, 3 at 288 K and four at other temperatures. Hence, 295 K has a significantly higher statistical weight than other temperatures. Since there is no meaningful justification for such

"over-weighting", tests 2–8 were performed with five 295 K records omitted. The records to omit were selected arbitrarily. For instance, in tests 7 and 8, the records with the shortest and longest τ, respectively, were omitted.

Further, we could use directly the τ values instead of $\Delta\tau$ (tests 9–12), or $\Delta\mathrm{STD} = 0.002$ rather than 0.001 (tests 13–16), or STD5 instead of STD100 (tests 17–28). In all cases, the results shown in table 3 correspond to the maximum deviation from test 1 within a given set of tests with various numbers of the data records at 295 K.

The results of these tests are summarized in the last row of table 3, which gives the ranges of E_a and τ_∞ obtained with the parameters of the reaction center from table 1.

A.4 Other sets of parameters

A total of 13 sets of parameters have been explored. We will review the most informative results and compare them with what has been obtained for Set IV. Some sets are shown in table 4.

We remind that only two adjustable static parameters, p and p_{cl}, are available to fit the experimental curves at low-temperatures where the calculated kinetics depends solely on these parameters but is independent of the relaxation time. We also said in Section 3.3 that it is more suitable to use $k_2(193)$ instead of p since the experimental value of this quantity can be utilized as a starting point.

Sets I–III are based on $k_2(193) = 0.154$, the average value for three experimental records at this temperature and variable $p_{cl} = 7 - 10$. The common feature of the calculated kinetics is higher STD100, which are increased by a factor of 1.2–1.5 at 193, 207, 223 and 238 K as compared to Set IV. As a result, the STD vs. τ dependences showed no minima for all records at 251 K, three records at 261 K and three records at 270 K. Therefore, these sets are unsatisfactory.

Set IV was obtained by increasing $k_2(193)$ by about two times, see table 1. We remind that k_2 is the second derivative of the kinetic curve at $t = 0$, equation (30). Therefore, increasing k_2 with respect to its experimental value should result in poorer agreement with experiment at short times. Indeed, STD5 characterizing the quality of the fits at the initial stage of the decay at times 0–5 μs are slightly increased, by about a few percent, as compared to Set III. However, as was said above, the overall agreement at the 100 μs interval is improved significantly. This is the reason to consider Set IV better than Set III.

The next trial was to increase $k_2(193)$ further. In Set XIII, we took $k_2(193) = 0.5$ keeping p_{cl} unchanged. The fitting results for kinetic curves at $T < 251$ K were significantly poorer than for Set IV since STD100 and STD5 increased by 15–35 and 15–60%, respectively.

Sets V–XII was built on varying p_{cl} at a given $k_2(193) = 0.3$. As discussed in Section 3.3, decreasing p_{cl} below the value for Set IV led to unrealistic values of the generic parameters. Therefore, only increased values were explored up to $p_{cl} = 100$. Some relevant sets are shown in table 4. It is seen that increasing p_{cl} results in a corresponding decrease of λ_q whereas other parameters change only slightly. Very small values of λ_q, say, less than 0.01 eV ($\approx 80\,\mathrm{cm}^{-1}$) are of little meaning. Therefore, further increase in p_{cl} was not considered.

No significant influence on the quality of the fits was achieved with these sets as compared to Set IV. The values of the activation energy were obtained in the range 0.46–0.57 eV for Set IX and 0.48–0.59 eV for Set XII.

B Solving the diffusion-reaction equation

It is appropriate to introduce new variables $\theta = t/\tau$ and y by equation (22) and rewrite equation (5) for P using equations (6) and (23),

$$\frac{\partial P}{\partial \theta} = \frac{1}{2}\frac{\partial^2 P}{\partial y^2} + y\frac{\partial P}{\partial y} + [1 - a\kappa(y)]P \tag{32}$$

where $a = k_0\tau/\sqrt{\alpha}$. The initial distribution at $\theta = 0$ is

$$P(y;0) = \frac{\exp(-y^2)}{\sqrt{\pi}} \tag{33}$$

Introducing a new unknown function $f(y, \theta)$,

$$P(y;\theta) = \sqrt{P(y;0)}f(y,\theta) \tag{34}$$

brings equation (32) into a self-adjoint form,

$$\frac{\partial f}{\partial \theta} = -[H(y) + a\kappa(y)]f \tag{35}$$

where

$$H(y) = -\frac{1}{2}\frac{\partial^2}{\partial y^2} + \frac{1}{2}y^2 - \frac{1}{2}$$

has the form of the Hamiltonian of the harmonic oscillator,

$$H(y) \equiv -\frac{\hbar^2}{2m}\frac{\partial^2}{\partial y^2} + \frac{1}{2}m\omega^2 y^2 + E_0$$

with $\hbar\omega = 1$, $m\omega^2 = 1$, $E_0 = -1/2$. The approximate solution to equation (35) is expanded in a finite, N-term series over the eigenfunctions of $H(y)$,

$$f(y;\theta) \equiv \sum_{n=0}^{N} f_n(\theta)\phi_n(y) \tag{36}$$

The eigenfunctions satisfy the equation $H\phi_n = n\phi_n$ and have the well-known form,

$$\phi_n(y) = \left(\sqrt{\pi}\,2^n n!\right)^{(-1/2)} \mathrm{e}^{(-1/2)y^2} H_n(y)$$

where $H_n(y)$ are the Hermite polynomials. The initial distribution, equation (33), can be rewritten as

$$P(y;0) \equiv \phi_0(y)^2 \tag{37}$$

Inserting equation (36) into equation (35), after multiplying with ϕ_n and integrating over y, we obtain

$$\frac{\partial f_n(\theta)}{\partial \theta} = -\sum_{n'=0}^{N} B_{nn'} f_{n'}(\theta) \tag{38}$$

where

$$B_{nn'} = n\delta_{nn'} + a\kappa_{nn'} \quad \kappa_{nn'} = \int_{-\infty}^{\infty} \phi_n(y)\kappa(y)\phi_{n'}(y)\mathrm{d}y$$

and $\delta_{nn'}$ is the Kroneker symbol. The survival probability is given by

$$Q(t) \equiv \int_{-\infty}^{\infty} P\left(y; \frac{t}{\tau}\right)\mathrm{d}y = f_0\left(\frac{t}{\tau}\right)$$

where we inserted equations (33), (34), (36) and (37) and used the fact that the eigenfunctions are orthogonal and normalized to unity. The differential equation (38) has to be solved with the initial condition

$$f_n(0) = \delta_{n0} \tag{39}$$

which follows from equations (34), (36) and (37). Next, we find the eigenvalues and eigenvectors of B,

$$\sum_{n'=0}^{N} B_{nn'} f_{n'}^{(k)} = \lambda_k f_n^{(k)}$$
$$\sum_{k=0}^{N} f_n^{(k)} f_{n'}^{(k)} = \delta_{nn'} \tag{40}$$

Using equation (40), it is easy to show that the solution to equation (38) obeying the initial condition (39) has the form

$$f_n(\theta) = \sum_{k=0}^{N} f_0^{(k)} f_n^{(k)}\, \mathrm{e}^{-\lambda_k \theta}$$

The final expressions for the survival probability and the distribution over y at time t are

$$Q(t) = \sum_{k=0}^{N} \left(f_0^{(k)}\right)^2 \mathrm{e}^{(-\lambda_k t/\tau)}$$

$$P\left(y; \frac{t}{\tau}\right) = \phi_0(y) \sum_{n=0}^{N} \phi_n(y) \sum_{k=0}^{N} f_0^{(k)} f_n^{(k)}\, \mathrm{e}^{(-\lambda_k t/\tau)}$$

In numerical calculations, 10 basis functions were used. Increasing N from 10 to 15 did not affect the calculated $Q(t)$ curves for the relaxation times $\tau = 0.001 - 1000\,\mu$s in the time interval $t = 0.1 - 100\,\mu$s.

References

[1] A.I. Kotelnikov, N.S. Goryachev, A.Y. Rubtsov, B.L. Psikha, X.M. Ortega. Analysis of the electron transfer kinetics in reaction centers from photosynthetic bacteria in frames of the Rips-Jortner model. *Dokl. Akad. Nauk*, **405**, 830 (2005), in Russian [English transl.: 2005. Doklady Biochemistry and Biophysics 405:461-464].

[2] A.I. Kotelnikov, J.M. Ortega, E.S. Medvedev, B.L. Psikha, D. Garcia, P. Mathis. Combined dynamic model for the kinetics of electron transfer from the cytochrome to a bacteriochlorophyll dimer in reaction centers of *Rps. sulfoviridis*. *Electrokhimiya*, **38**, 90 (2002).

[3] A.I. Kotelnikov, J.M. Ortega, E.S. Medvedev, B.L. Psikha, D. Garcia, P. Mathis. Effect of protein relaxation on electron transfer from the cytochrome subunit to the bacteriochlorophyll dimer in Rps. sulfoviridis reaction centers within mixed adiabatic/non-adiabatic model. *Bioelectrochemistry*, **56**, 3 (2002).

[4] J.M. Kriegl, G.U. Nienhaus. Structural, dynamic, and energetic aspects of long-range electron transfer in photosynthetic reaction centers. *Proc. Natl. Acad. Sci. USA*, **101**, 123 (2004).

[5] B.H. McMahon, J.D. Müller, C.A. Wraight, G.U. Nienhaus. Electron transfer and protein dynamics in the photosynthetic reaction center. *Biophys. J.*, **74**, 2567 (1998).

[6] J.C. Lee, H.B. Gray, J.R. Winkler. Tertiary Contact Formation in r-Synuclein Probed by Electron Transfer. *J. Am. Chem. Soc.*, **127**, 16388 (2005).

[7] J.C. Lee, I.-J. Chang, H.B. Gray, J.R. Winkler. The cytochrome c folding landscape revealed by electron-transfer kinetics. *J. Mol. Biol.*, **320**, 159 (2002).

[8] I.-J. Chang, J.C. Lee, J.R. Winkler, H.B. Gray. The protein-folding speed limit: Intrachain diffusion times set by electron-transfer rates in denatured $Ru(NH_3)5$(His-33)-Zn-cytochrome c. *Proc. Natl. Acad. Sci. USA*, **100**, 3838 (2003).

[9] J.R. Winkler, P. Wittung-Stafshede, J. Leckner, B.G. Malmstrom, H.B. Gray. Effect of folding on mettalloprotein active sites. *Proc. Natl. Acad. Sci. USA*, **94**, 4246 (1997).

[10] J.R. Telford, P. Wittung-Stafshede, H.B. Gray, J.R. Winkler. Protein folding triggered by electron transfer. *Acc. Chem. Res.*, **31**, 755 (1998).

[11] C.C. Moser, J.M. Keske, K. Warncke, R.S. Farid, P.L. Dutton. Nature of Biological electron transfer. *Nature*, **355**, 796 (1992).

[12] H.B. Gray, J.R. Winkler. Electron transfer in proteins. *Annu. Rev. Biochem.*, **65**, 537 (1996).

[13] H. Sumi, R.A. Marcus. Dynamical effects in electron transfer reactions. *J. Chem. Phys.*, **84**, 4894 (1986).

[14] L.D. Zusman. Outersphere electron transfer in polar solvents. *Chem. Phys.*, **49**, 295 (1980).

[15] M.Y. Ovchinnikova. On the frequency factor in the rate constant of the electron transfer reaction. *Teor. Eksp. Khim.*, **17**, 651 (1981).

[16] I.V. Alexandrov. Physical aspects of charge transfer theory. *Chem. Phys.*, **51**, 449 (1980).

[17] A.B. Helman. The effect of intramolecular modes on the velocity of nonradiative transitions in a polar medium. *Chem. Phys.*, **65**, 271 (1982).

[18] N. Agmon, J.J. Hopfield. CO binding to heme proteins: A model for barrier height distributions and slow conformational changes. *J. Chem. Phys.*, **79**, 2042 (1983).

[19] I. Chang, H. Hartmann, Y. Krupyanskii, A. Zharikov, F. Parak. Dielectric relaxation models applied to the dynamics of myoglobin as determined by Mossbauer spectroscopy. *Chem. Phys.*, **212**, 221 (1996).

[20] E.N. Frolov, V.I. Goldanskii, A. Birk, F. Parak. The influence of electrostatic interactions and intramolecular dynamics on electron transfer from the cytochrome subunit to the cation-radical of the bacteriochlorophyll dimer in reaction centers from *Rps. viridis*. *Eur. Biophys. J.*, **24**, 433 (1996).

[21] A.I. Kotelnikov. *Unpublished results*.

[22] A.V. Pastukhov, V.R. Fogel, A.I. Kotelnikov, D.V. Khudyakov, B.L. Psikha. Dynamics of spectral relaxation of phosphorescence of eosin in overcooled water-ethylene glycol solutions. *Opt. Spectrosc.*, **86**, 363 (1999).

[23] A.V. Pastukhov, D.V. Khudyakov, V.R. Fogel, A.I. Kotelnikov. A supercooled glucerol-water mixture: evidence for the large-scale heterogeneity?. *Chem. Phys. Lett.*, **346**, 6168 (2001).

[24] J.S. Bashkin, G. McLendon, S. Mukamel, J. Marohn. Influence of medium dynamics on solvation and charge separation reactions: Comparison of a simple alcohol and a protein "solvent". *J. Phys. Chem.*, **94**, 4757 (1990).

[25] E. Lee, E.S. Medvedev, A.A. Stuchebrukhov. Effect of quantum modes in biological electron transfer reactions: A useful approximation for the harmonic model with frequency change and Duchinsky rotation. *J. Chem. Phys.*, **112**, 9015 (2000).

[26] I. Daizadeh, E.S. Medvedev, A.A. Stuchebrukhov. Effect of protein dynamics on biological electron transfer. *Proc. Natl. Acad. Sci. USA*, **94**, 3703 (1997).
[27] E.S. Medvedev, A.A. Stuchebrukhov. Inelastic tunneling in long-distance biological electron transfer reactions. *J. Chem. Phy.*, **107**, 3821 (1997).
[28] E.S. Medvedev, A.A. Stuchebrukhov. Dynamic effects in long-distance biological electron transfer reactions. *Pure Appl. Chem.*, **70**, 2201 (1998).
[29] H. Nishioka, A. Kimura, T. Yamato, T. Kawatsu, T. Kakitani. Interference, fluctuation, and alternation of electron tunneling in protein media. 1. Two tunneling routes in photosynthetic reaction center alternate due to thermal fluctuation of protein conformation. *J. Phys. Chem. B*, **109**, 1978 (2005).
[30] H. Nishioka, A. Kimura, T. Yamato, T. Kawatsu, T. Kakitani. Interference, fluctuation, and alternation of electron tunneling in protein media. 2. Non-condon theory for the energy gap dependence of electron transfer rate. *J. Phys. Chem. B*, **109**, 15621 (2005).
[31] T. Kawatsu, T. Kakitani, T. Yamato. Destructive interference in the electron tunneling through protein media. *J. Phys. Chem. B*, **106**, 1135611366 (2002).
[32] I.A. Balabin, J.N. Onuchic. Dynamically controlled protein tunneling paths in photosynthetic reaction centers. *Science*, **290**, 114 (2000).
[33] A. Vermeglio, D. Garcia, J. Breton. Cytochrome arrangements in reaction centers of different species of photosynthetic bacteria. In *Reaction Centers of Photosynthetic Bacteria*, M.E. Michel-Beyerle (Ed.), Vol. 6, pp. 19–22, Springer-Verlag, Berlin (1989).
[34] J.M. Ortega, P. Mathis. Electron transfer from tetraheme cytochrome to the special pair in isolated reaction centers of *Rhodopseudomonas viridis*. *Biochemistry*, **32**, 1141 (1993).
[35] J.M. Ortega, P. Mathis. Effect of temperature on the kinetics of electron transfer from the tetraheme cytochrome to the primary donor in *Rhodopseudomonas viridis*. *FEBS Lett.*, **301**, 45 (1992).
[36] J.M. Ortega, B. Dohse, D. Oesterhelt, P. Mathis. Very fast electron transfer from cytochrome to the bacterial photosynthetic reaction center. *FEBS Lett.*, **401**, 153 (1997).
[37] J.M. Ortega, B. Dohse, D. Oesterhelt, P. Mathis. Low-temperature electron transfer from cytochrome to the special pair in *Rhodopseudomonas viridis*. *Biophys. J.*, **74**, 1135 (1998).
[38] R.J. Shopes, C.A. Wraight. Charge recombination from the P+QA- state in reaction centers from *Rhodopseudomonas viridis*. *Biochim. Biophys. Acta*, **893**, 409 (1987).
[39] W. Nadler, R.A. Marcus. Dynamical effects in electron transfer reactions. II. Numerical solution. *J. Chem. Phys.*, **86**, 3906 (1987).
[40] B. Bagchi, G.R. Fleming, D.W. Oxtoby. *J. Chem. Phys.*, **78**, 7375 (1983).
[41] G.U. Nienhaus, H. Frauenfelder, F. Parak. Structural fluctuations in glass-forming liquids: Mossbauer spectroscopy on iron in glycerol. *Phys. Rev. B*, **43**, 3345 (1991).
[42] J.R. Huck, G.A. Noyel, L. Jorat. Dielectric properties of supercooled glycerol-water solutions. *J. IEEE Trans. Elect. Insul.*, **23**, 627 (1988).